IOP Publishing Nanotechnology
Nanotechnology 20 (2009) 035706 (6pp) doi:10.1088/0957-4484/20/3/035706

Elastic moduli of faceted aluminum nitride nanotubes measured by contact resonance atomic force microscopy

G Stan[1], C V Ciobanu[2], T P Thayer[2], G T Wang[3], J R Creighton[3], K P Purushotham[4], L A Bendersky[5] and R F Cook[1]

[1] Ceramics Division, National Institute of Standards and Technology, Gaithersburg, MD 20899, USA
[2] Division of Engineering, Colorado School of Mines, Golden, CO 80401, USA
[3] Advanced Materials Sciences Department, Sandia National Laboratories, Albuquerque, NM 87185, USA
[4] Precision Engineering Division, National Institute of Standards and Technology, Gaithersburg, MD 20899, USA
[5] Metallurgy Division, National Institute of Standards and Technology, Gaithersburg, MD 20899, USA

E-mail: gheorghe.stan@nist.gov and cciobanu@mines.edu

Received 25 August 2008, in final form 24 October 2008
Published 17 December 2008
Online at stacks.iop.org/Nano/20/035706

Abstract
A new methodology for determining the radial elastic modulus of a one-dimensional nanostructure laid on a substrate has been developed. The methodology consists of the combination of contact resonance atomic force microscopy (AFM) with finite element analysis, and we illustrate it for the case of faceted AlN nanotubes with triangular cross-sections. By making precision measurements of the resonance frequencies of the AFM cantilever-probe first in air and then in contact with the AlN nanotubes, we determine the contact stiffness at different locations on the nanotubes, i.e. on edges, inner surfaces, and outer facets. From the contact stiffness we have extracted the indentation modulus and found that this modulus depends strongly on the apex angle of the nanotube, varying from 250 to 400 GPa for indentation on the edges of the nanotubes investigated.

(Some figures in this article are in colour only in the electronic version)

1. Introduction

Aluminum nitride has an intriguing combination of physical properties, such as enhanced field emission, large optical band gap, high thermal conductivity, large electrical resistivity, as well as a piezoelectric coefficient comparable to that of quartz. These properties make AlN nanostructures suitable for advanced nanoscale electronic and optoelectronic device applications, and have motivated sustained efforts to synthesize AlN nanostructures in various morphologies: wires [1, 2], nanoparticles [3], nanotubes [4], needles [5], and platelets [6]. While many applications for AlN nanostructures target their use as field emitters in flat panel displays, their superior piezoelectric properties and integration compatibility with silicon substrates make them excellent candidates for sensors, actuators, and nano-electromechanical systems (NEMS) [7, 8]. Given the diversity in morphology, cross-section, and size resulting from current synthesis methods [1–6, 9, 10], the properties of one-dimensional (1D) AlN nanostructures that are important for the fabrication and performance of NEMS, in particular mechanical properties, can be rather difficult to quantify. This difficulty is due to size-dependent effects at the nanoscale, large surface-to-volume ratio, and the possible presence of defects acquired during the nanostructure growth process. Furthermore, in the current indentation-based methods used to measure the elastic properties of AlN bulk single crystals (e.g., [11]) the sensing indentation depths are on the order of hundreds nanometers. This means that such methods cannot be used to measure the elastic

 © 2009 IOP Publishing Ltd Printed in the UK

properties of AlN nanostructures, critical to NEMS design and performance, that have diameters comparable to the typical indentation depths. It is therefore necessary to design procedures to accurately determine the elastic properties of 1D AlN structures, particularly methods that can locally probe the variation of elastic moduli along an axis and in various locations on a cross-section.

Here, we report experimental measurements of local elastic properties of faceted AlN nanotubes (AlN NTs) with triangular cross-section by contact resonance atomic force microscopy (CR-AFM) [12, 13]. The AlN NTs were obtained from core–shell GaN–AlN nanowires after thermally removing the GaN cores, which is a novel procedure for synthesizing NTs with controllable wall thickness [14]. We characterized the AlN NTs using a suite of microscopy techniques to determine their crystallography and geometric dimensions. Next, we performed CR-AFM measurements on AlN NTs to determine the stiffness of the contact formed between the atomic force microscope (AFM) tip and the NTs. As the contact stiffness depends on *both* the elastic properties of the materials and the contact geometry, it cannot be readily mapped onto an indentation modulus value of an AlN NT. We therefore performed finite element analysis (FEA) calculations in order to account for the actual experimental contact geometry and to convert the contact stiffness into a unique value for the indentation modulus of the NT. Due to the combination with FEA simulations for realistic geometries, our procedure to determine the elastic properties breaks away from the usual analysis based on Hertzian contact models and is applicable in general for 1D nanostructures of *any* cross-sectional shape, potentially yielding the radial elastic modulus at any location along a substrate-supported nanowire or nanotube. Such local probing gives accurate values of the elastic moduli of 1D nanostructures, and can also reveal the presence of defects via variations of these moduli.

2. AlN nanotubes: synthesis and morphology

The AlN NTs in our study were synthesized through an 'epitaxial casting' process similar to that reported previously for the synthesis of GaN nanotubes [14]. Using triangular-faceted GaN nanowires synthesized by Ni-catalyzed metal–organic chemical vapor deposition (MOCVD) [15] at 800 °C, AlN shells were grown around the GaN nanowires by MOCVD at 1000 °C [16]. The GaN cores were subsequently removed by annealing in hydrogen atmosphere at 1120 °C for approximately 3 h, leaving behind the empty AlN shells. The AlN NTs so obtained were harvested and dispersed onto Au films, Cu grids, and Si substrates for various microscopy measurements. The structure and morphology of AlN NTs were investigated by means of scanning electron microscopy (SEM), transmission electron microscopy (TEM), and AFM. Each technique indicated that the AlN NTs were hollow prisms with rounded edges that preserved the triangular cross-section of the GaN core templates. Such triangular cross-sections are shown in SEM images in figures 1(a)–(c). The crystallographic structure of the NTs was established from TEM images and their corresponding selected-area electron diffraction (SAED)

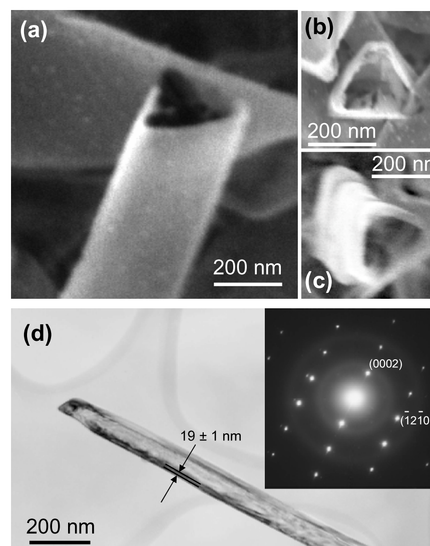

Figure 1. (a)–(c) SEM images of faceted AlN nanotubes, in lateral (a) and axial views ((b), (c)). The images clearly show that the nanotube cross-sections are triangular, with the side of the triangles of the order of 200 nm. (d) TEM image of an AlN NT grown along the [$\bar{1}2\bar{1}0$] direction. The thickness of the nanotube walls was estimated at 19 ± 1 nm. From the corresponding SAED pattern (shown in inset), distances between crystalline planes were determined to be 0.25 nm and 0.15 nm for the (0002) and the ($\bar{1}2\bar{1}0$) families of planes, respectively. These distances are consistent with the AlN lattice constants $c = 0.498$ and $a = 0.311$ nm [17].

patterns, which show that the NTs were predominately single crystals of wurtzite structure with the ⟨$\bar{1}2\bar{1}0$⟩ growth direction (figure 1(d)). The measured lattice parameters fit well the wurtzite structure of AlN [17]. Observed intensity streaks in the [0001] direction of [$01\bar{1}0$] SAED pattern in the inset of figure 1(d) suggest that one of the tube facets is a (0001) plane. Consequently, the facets forming the triangular tubular prisms are the planes (0001), ($10\bar{1}1$), and ($\bar{1}011$). This configuration is similar to that of GaN nanowires [15, 18] grown under similar conditions to the removed GaN cores in our work. The wall thickness of the NTs was measured as 19 ± 1 nm from the thickness fringes that shadow the tube walls in TEM images. A wall thickness of 20 ± 1 nm was measured on tube walls exposed parallel to the electron beam in SEM. The SEM images were taken with a FEI Helios dual-beam microscope[6] at an accelerating voltage of 15 kV and a beam current of 86 pA. The TEM images were acquired on a JEOL JEM-3010 transmission electron microscope at 300 kV.

3. CR-AFM measurements on AlN nanotubes

To quantify the elastic properties of the AlN NTs, we have employed the CR-AFM technique [12, 13] adapted for 1D nanostructures axially supported on surfaces [19, 20]. In this

[6] Certain commercial equipment, instruments, or materials are identified in this document. Such identification does not imply recommendation or endorsement by the National Institute of Standards and Technology, nor does it imply that the products identified are necessary the best available for the purpose.

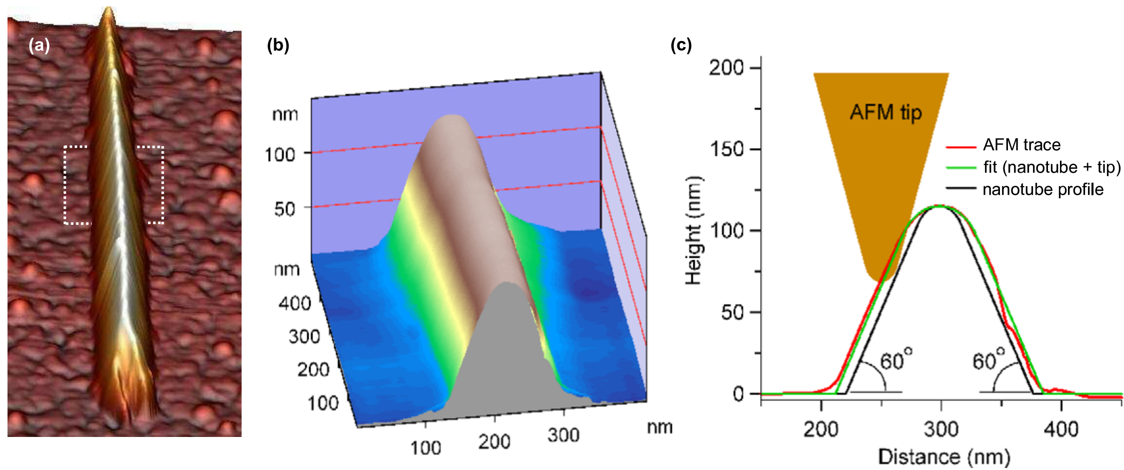

Figure 2. (a) AFM image of a long AlN NT. (b) Detailed AFM profile of the 500 nm nanotube segment highlighted in (a). (c) Averaged AFM trace (red curve) of the profile shown in (b), which was used to extract the shape of the AlN NT via an erosional fit (green curve). The resulting nanotube profile (black curve) is characterized by 60° basal angles and a rounded apex with a radius of 20 nm.

technique, the stiffness $k^{\star}$ of the contact formed between an AFM tip and a nanotube is determined from the shift in the cantilever's resonance frequencies measured when the tip is brought from air into contact with the AlN NT. The contact stiffness is then used to calculate the indentation modulus of the NT sample, M_{NT}, by means of the Hertz contact formula [21]:

$$k^{\star} = 2a\frac{M_{\mathrm{NT}}M_{\mathrm{t}}}{M_{\mathrm{NT}}+M_{\mathrm{t}}}, \qquad (1)$$

where a is the contact radius, and M_{NT} and M_{t} are the indentation moduli of the NT sample and the tip, respectively. The indentation moduli for isotropic materials have simple expressions in terms of Young's modulus E and Poisson's ratio ν, e.g., $M_{\mathrm{NT}} = E_{\mathrm{NT}}/(1-\nu_{\mathrm{NT}}^2)$; anisotropy corrections to the indentation modulus may also be evaluated [23, 22]. Equation (1) implies that in order to calculate the indentation modulus M_{NT} from the contact stiffness $k^{\star}$ it is necessary to have knowledge of the contact geometry, i.e. of the contact radius a.

CR-AFM measurements were performed on a commercial AFM (Veeco MultiMode III, Santa Barbara CA) with additional instrumentation (LabView, National Instruments, Austin, TX) (see footnote 6). A lock-in amplifier with internal signal generator (7280 Signal Recovery AMETEK, Oak Ridge, TN) was used to induce vibrations in the AFM cantilever and to collect the high-frequency signal from the photodiode detector [35]. The AFM probes (PPP-SEIH NanoSensors, Neuchatel, Switzerland) used in this work were single-crystal Si cantilevers with [100]-oriented tips. The cantilever stiffness k_{c} was determined to be 11.5 ± 0.5 N m^{-1} by the thermal-noise method [36]. A constant applied load F of about 200 nN was applied in each measurement. The applied load (kept constant throughout the measurements) was much greater that the adhesion force between the tip and surface while small enough that the contact deformations are in the linear elastic regime.

Taking advantage of the spatial resolution allowed by CR-AFM, we have made elastic modulus measurements at

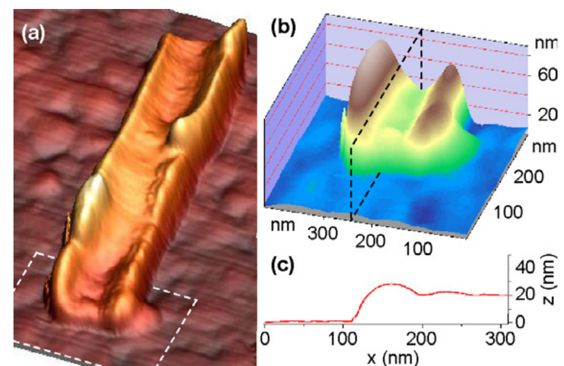

Figure 3. Thickness of AlN NT walls determined from AFM measurements of a nanotube sectioned along its axis. (a) AFM image of a micrometer-long nanotube. (b) Detailed profile of the end portion of the tube (dashed-line contour in (a)). (c) Line profile obtained with the tip moved in the axial plane highlighted in (b); the wall thickness is found to be 20 ± 1 nm.

different locations on AlN NTs: on top edges of a few tubes laid down on the substrate (one of these measured tubes is shown in figure 2), on an outer nanotube facet positioned parallel to the substrate (not shown here), and on the inside facet of a broken tube (shown in figure 3). The parameters necessary to resolve the geometry of the contact between the tip and the round top edge of the prismatic NTs were determined from topographical AFM scans of the AlN NTs. Figures 2(a) and (b) show detailed 3D AFM topographies of a sample prismatic AlN nanotube. The average cross-section of the AFM trace shown in figure 2(b) was used to construct the outer profile of the nanotube in figure 2(c) by subtracting the contribution of the tip from the AFM trace. The angles formed by the side facets of the AlN NT with the substrate are not affected by the tip's contribution to the AFM image (figure 2(c)). For the case shown in figure 2(c) these basal angles were found to be $\simeq 60°$, indicating a cross-section similar to that formed by the crystallographic planes (0001), $(10\bar{1}1)$, and $(\bar{1}011)$ of the wurtzite structure. Deviations less

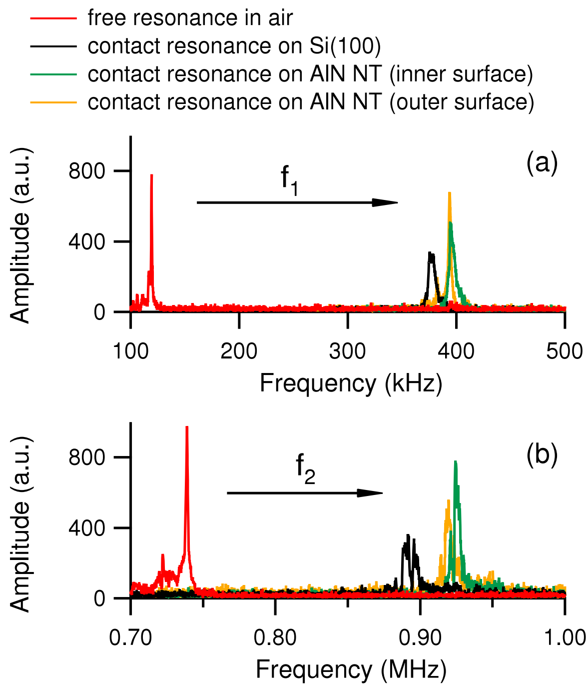

Figure 4. The shifts of (a) first and (b) second resonance frequencies measured when the AFM tip is brought from air into contact with a Si(100) reference surface (black curves), with the inner surface of a sectioned tube (green curves), and with an outer facet of AlN NTs (orange curves).

than 10° were observed for the facet angles for all AlN NTs investigated. The round top edge observed in AFM scans (see figure 2), had a curvature radius determined to be 20 nm.

For each tested AlN NT, the contact stiffness $k^{\star}_{\mathrm{NT}}$ was calculated (in terms of the cantilever stiffness k_{c}) from the first two contact resonance frequencies, $f_{1,\mathrm{NT}}$ and $f_{2,\mathrm{NT}}$, measured in five CR-AFM frequency sweeps. Figure 4 shows the shifts in CR-AFM frequencies when the cantilever was moved from air into contact with the AlN NTs flat facets, as well as onto a Si(100) reference surface. By tuning the applied load, we have ensured an increased sensitivity of the contact resonance frequencies to variations in the elastic properties of the materials tested. For the resonances shown in figure 4, the system behaved as a clamped-spring coupled beam rather than a clamped–clamped beam, i.e., the ratio of the first contact resonance frequency to the first free resonance frequency of the cantilever was smaller than 4 (this ratio is about 5 in the case of clamped–clamped cantilever beam) [12]. On a given NT sample, the average values of the two contact resonance frequencies were used in a clamped-spring coupled beam model [12] of the cantilever to uniquely determine the contact stiffness $k^{\star}_{\mathrm{NT}}$. The geometry of the contact plays a significant role in extracting the elastic modulus of the sample tested from the contact stiffness. In particular, a substantial change in the contact area occurs when CR-AFM measurements on the top edge of prismatic AlN nanotubes have to be calibrated to those made on a flat Si(100) surface. The contact geometries for the tip in contact with the reference Si(100) surface and the tip on the nanotube edge are shown schematically in figures 5(a) and (b), respectively. The procedure to account for the contact

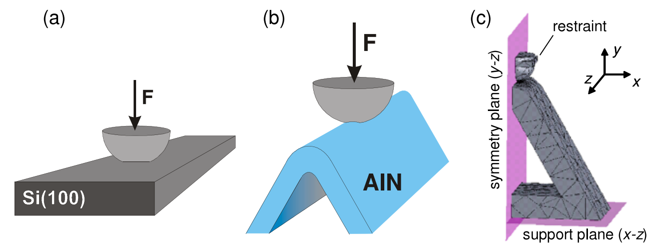

Figure 5. Geometric configuration of the contact between (a) tip-on-flat Si(100) surface and (b) tip-on-prismatic edge of AlN nanotube. Under the same applied force, the contact area is circular in (a) and elliptical in (b). (c) Schematic geometry used in FEA calculations. The points on the x–z support plane of the triangular nanotube have z-component of the displacements set to zero, and a restraint is placed on the hemispherical tip to prevent it from slipping along the nanotube surface. To speed up calculations, we exploit the symmetry of the system about the y–z plane by setting to zero the x-displacements of the points on this plane.

geometry and to extract the elastic modulus M_{NT} from the contact stiffness $k^{\star}_{\mathrm{NT}}$ is detailed below.

4. Elastic modulus of faceted AlN nanotubes

Using the geometry of the nanotube and the radius of the AFM tip derived from the AFM trace (refer to figure 2), FEA was performed to determine the load, F, versus displacement, δ, curve for radial indentation of the AlN NTs. We have used the FEA package Nastran/Patran (MSC Software Corp.) and solved the equations of elasticity with an adaptive mesh to improve convergence. We have started the FEA calculations with *uniform* meshes that have 3000–5000 tetragonal elements and up to 10 000 nodes. During FEA calculations, the adaptive mesh becomes finer in the high-stress contact region and coarser far away form it, as shown in figure 5(c). For clarity of the visualization, in figure 5(c) we show an intermediate stage of the calculation where it is apparent that the mesh has become denser in the contact region. We have replaced the substrate that supports the nanowire with rigid boundary conditions (refer to figure 5(c)), which is justified because, for the loads considered here, stresses decay rapidly with the distance from the contact point and become negligible in the vicinity of the supporting substrate. The tip was constrained to move only vertically, so as not to slip on the nanotube during the FEA calculation. Lastly, in order to speed up the solution we have taken advantage of the symmetry across the y–z plane (figure 5(c)) by setting the lateral displacements (i.e. along the x direction) to zero on that plane.

The displacement of the tip in the FEA calculations was recorded for each value of the applied load. For loads smaller than 500 nN and indentation moduli of the AlN NT assumed to be in the range 200 GPa $< M_{\mathrm{NT}} <$ 500 GPa, FEA calculation showed that the displacement of the AFM tip in contact with the AlN NT is proportional to $F^{2/3}$; apart from multiplicative factors that depend on the nanotube geometry and elastic modulus, this is the same dependence as that for Hertzian contact [21]. Consequently, the contact stiffness (defined as $k^{\star}_{\mathrm{NT}} = \partial F/\partial\delta$) is proportional to $F^{1/3}$. As the

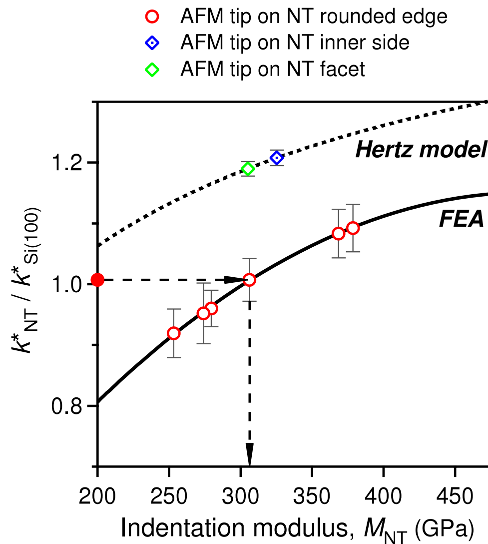

Figure 6. Determination of the indentation modulus M_{NT} of AlN nanotubes from CR-AFM measurements. The shifts in resonance frequencies set the ratio $k^\star_{NT}/k^\star_{Si(100)}$ (e.g., red solid dot on the vertical axis), which used in conjunction with the FEA-calculated dependence (solid curve) gives the indentation modulus of that nanotube (i.e. the M_{NT} coordinate of the open circles). A similar procedure has been applied for the contact between the AFM tip and flat surfaces of the AlN NTs, for which we have used the Hertz contact model formula [21] (dashed curve) instead of the FEA-calculated dependence.

stiffness $k^\star_{Si(100)}$ of the contact between the AFM tip and the flat Si(100) surface (taken as Hertzian) is also proportional to $F^{1/3}$, it follows that the ratio $k^\star_{NT}/k^\star_{Si(100)}$ is independent of load and can thus be plotted as a function of the indentation modulus of the NT. This FEA dependence is shown in figure 6 for a typical set of geometric parameters, i.e. tip radius of 15 nm, basal angle of the nanotube facet of 60°, nanotube wall thickness of 20 nm, and radius of curvature at the top of the AlN NT of 20 nm. These values are representative for our experiment and allow us to draw conclusions about the elastic properties of AlN NTs. FEA calculations can yield extensive families of curves for different tip radii, NT basal angles and wall thicknesses, and such families of curves can be used to refine the elastic moduli results; this refinement, however, is only necessary for nanotubes with much smaller radial dimensions than those synthesized in our experiments. For a given elastic modulus, the stiffness of the tip–tube contact always lies below of the stiffness of the tip–flat contact (figure 6) because of the increased structural compliance of the tube compared to that of a flat slab of the same size. The FEA stiffness ratio curve is the key to estimating the elastic modulus of the AlN NT, because a given stiffness ratio $k^\star_{NT}/k^\star_{Si(100)}$ as determined from resonance frequency measurements corresponds, via the FEA curve, to a unique value for the indentation modulus of the AlN NT (figure 6).

Using the FEA dependence, we have found that the indentation modulus M_{NT} for the rounded edges of the AlN NTs falls in the range 250–400 GPa, depending on the geometrical parameters of the tubes investigated. We note that the NTs with the greatest basal angle (refer to figure 6 and table 1) had the greatest indentation modulus, indicative of a size-dependent effect in which this modulus increases with decreasing apex angle at the rounded edge of the AlN NT. However, variations in the cross-sectional dimensions (sides, angles) of the NTs prevent us from making a more definite connection between M_{NT} and the apex angle; the wall thickness and the apex radius would necessarily enter into any size-dependence of M_{NT}. Another factor that could contribute to variations of the measured M_{NT} is the roughness on the core surfaces, which has been observed on the GaN nanowires [16]. Since the core has rough surfaces, it is expected that the AlN shell has rough or defected surfaces too. To release the mismatch strain between AlN and GaN, threading dislocations may also form at the core–shell interface during the growth of the shell as observed in thin-film systems [24]. While some of these dislocations may be annealed away during the core removal, it is unlikely for the remaining AlN shell to be dislocation-free.

Table 1. Indentation modulus M_{NT} for selected AlN NTs, as determined by CR-AFM measurements with the AFM tip in contact with the nanotube apex. The NTs have isosceles triangle cross-sections with rounded apices, and are characterized by the angle α of a lateral facet with the substrate and the height h. The last two rows of the table show the indentation modulus measured on an inner and outer flat surfaces of the AlN nanotubes.

Angle α (deg)	Height h (nm)	M_{NT} (GPa)
60.0	115	274.0 ± 29.5
60.5	88	279.5 ± 18.1
62.5	104	306.2 ± 23.7
64.5	198	253.3 ± 21.7
66.5	181	378.5 ± 36.8
69.0	127	372.1 ± 38.9
Inner NT facet		325.2 ± 15.5
Flat NT facet		305.0 ± 12.7

Interestingly, despite the presence of possible defects, the range of measured M_{NT} values includes the theoretical values for the indentation modulus of bulk single-crystal AlN of 300 GPa (indentation perpendicular to c-axis) and 335 GPa (indentation parallel to c-axis), which have been calculated using the elastic constants for AlN given in [25]. We also determined the stiffness ratio associated with the flat surfaces of the NTs, which can expose an inner side (figure 3) or an outer facet parallel to the substrate (not shown). For the indentation of flat facets, the FEA curve can be replaced by the exact analytic formula from the Hertz model (dashed-line curve in figure 6). The indentation moduli of AlN NT facets were found to be 305 GPa (outer facets) and 325 GPa (inner side), in good agreement with the theoretical values listed above. The indentation modulus values for flat facets are also included in table 1. In contrast to the case of nanowires, where the elastic modulus depends on their diameter [19, 20, 26, 27], no significant deviation from bulk value was observed here for the out-of-plane modulus of AlN facets as thin as 20 nm.

5. Conclusions

We have synthesized AlN NTs by an epitaxial casting process in which AlN was deposited on GaN triangular cores.

The cores were subsequently removed by annealing in a hydrogen atmosphere, and the resulting AlN NTs have been characterized by SEM, AFM, and TEM. We have investigated the radial elastic moduli of the AlN NTs laid down on a substrate using a combination of CR-AFM measurements and FEA calculations. Our approach complements a class of techniques for probing elastic properties of 1D nanostructures, which include *in situ* electromechanical resonance [28], bending tests [29–31], static and dynamic nanoindentation [32, 33], and tensile stress measurements [34].

The CR-AFM technique is based on measuring the shifts in resonant frequencies when the AFM tip is brought from air in contact with the sample, and from these frequency shifts we have calculated the stiffness associated with the contact between the AFM tip and nanotube tested. The FEA calculations enable us to use the contact stiffness to extract the indentation modulus of the AlN NTs for different contact geometries. The values that we determined for indentation modulus depend on the nanotube dimensions, but remain close to those of bulk AlN (300–335 GPa) [25] for most NTs investigated. For AlNTs with 20 nm thick walls, the indentation moduli corresponding to the inner surfaces and outer facets are determined to be 325 GPa and 305 GPa, respectively. Therefore, we have found that the reduction in size (a requirement for NEMS applications) does not imply a significant distortion of the mechanical properties of AlN NTs compared to those of bulk AlN. It is conceivable, however, that a moderate variation in the mechanical properties of AlN NTs synthesized through the 'epitaxial casting' process may be achieved by selecting GaN NWs templates with different cross-sections and different effective diameters.

We note that the approach presented here is general, and can be used for nanowires or nanotubes made of any material to determine the radial indentation modulus at any location on their outer surface. The only prerequisite for such general use is the ability to correctly characterize the shape and dimensions of the cross-section, which can be achieved straightforwardly by AFM for nanostructures as thin as 10 nm in diameter.

Acknowledgments

G T Wang acknowledges support from the DOE Office of Basic Energy Sciences and Sandia's Laboratory Directed Research and Development program. Sandia is a multiprogram laboratory operated by Sandia Corporation, a Lockheed Martin Company, for the United States Department of Energy's National Nuclear Security Administration under contract No. DE-AC04-94Al85000.

References

[1] Haber J A, Gibbons P C and Buhro W E 1998 *Chem. Mater.* **10** 4062
[2] Zhang Y, Liu J, He R, Zhang Q, Zhang X and Zhu J 2001 *Chem. Mater.* **13** 3899
[3] Haoa X P, Yub M Y, Cuia D L, Xua X G, Baia Y J, Wangb Q L and Jianga M H 2002 *J. Cryst. Growth* **242** 229
[4] Tondare V N, Balasubramanian C, Shende S V, Joag D S, Godbole V P, Bhoraskara S V and Bhadbhade M 2002 *Appl. Phys. Lett.* **80** 4813
[5] Zhao Q, Xu J, Xu X Y, Wang Z and Yu D 2004 *Appl. Phys. Lett.* **85** 5331
[6] Tang Y B, Cong H T and Cheng H M 2006 *Appl. Phys. Lett.* **89** 093113
[7] Cleland A N, Pophristic M and Fergusson I 2001 *Appl. Phys. Lett.* **79** 2070
[8] Cimalla V *et al* 2007 *Sensors Actuators* B **126** 24
[9] Wu Q, Hu Z, Wang X, Lu Y, Chen X, Xu H and Chen Y 2003 *J. Am. Chem. Soc.* **125** 10176
[10] Yin L W, Bando Y, Zhu Y C, Li M S, Tang C C and Golberg D 2005 *Adv. Mater.* **17** 213
[11] Yonenaga I, Shima T and Sluiter M H F 2002 *Japan. J. Appl. Phys.* **41** 4620
[12] Rabe U, Janser K and Arnold W 1996 *Rev. Sci. Instrum.* **67** 3281
[13] Yamanaka K and Nakano S 1996 *Japan. J. Appl. Phys.* **35** 3787
[14] Goldberger J, He R, Zang Y, Lee S, Yan H, Choi H and Yang P D 2003 *Nature* **422** 599
[15] Wang G T, Talin A A, Werder D J, Creighton J R, Lai E, Anderson R J and Arslan I 2006 *Nanotechnology* **17** 5773
[16] Arslan I, Talin A A and Wang G T 2008 *J. Phys. Chem.* C **112** 11093
[17] Iwama S, Hayakawa K and Arizumi T 1982 *J. Cryst. Growth* **56** 265
[18] Li Q and Wang G T 2008 *Appl. Phys. Lett.* **93** 043119
[19] Stan G, Ciobanu C V, Parthangal P M and Cook R F 2007 *Nano Lett.* **7** 3691
[20] Stan G, Krylyuk S, Davydov A V, Vaudin M, Bendersky L A and Cook R F 2008 *Appl. Phys. Lett.* **92** 241908
[21] Johnson K L 1985 *Contact Mechanics* (Cambridge: Cambridge University Press)
[22] Kumar A, Rabe U, Hirsekorn S and Arnold W 2008 *Appl. Phys. Lett.* **92** 183106
[23] Vlassak J J and Nix W D 1993 *Phil. Mag.* A **67** 1045
[24] Sang L W, Qin Z X, Fang H, Zhou X R, Yang Z J, Shen B and Zhang G Y 2008 *Appl. Phys. Lett.* **92** 192112
[25] Tsubouchi K, Sugai K and Mikoshiba N 1981 *1981 Ultrasonics Symp.* vol I, ed B R McAvoy (New York: IEEE) p 375
[26] Cuenot S, Fretigny C, Demoustier-Champagne S and Nysten B 2004 *Phys. Rev.* B **69** 165410
[27] Chen C Q, Shi Y, Zhang Y S, Zhu J and Yan Y J 2006 *Phys. Rev. Lett.* **96** 075505
[28] Poncharal P, Wang Z L, Ugarte D and de Heer W A 1999 *Science* **283** 1513
[29] Salvetat J P, Kulik A J, Bonard J M, Briggs G A D, Stockli T, Motonier K, Bonnamy S, Boguin F, Burnham N A and Forro L 1999 *Adv. Mater.* **11** 161
[30] Wu B, Heidelberg A and Boland J J 2005 *Nat. Mater.* **4** 525
[31] Song J H, Wang X D, Riedro E and Wang Z L 2005 *Nano Lett.* **5** 1954
[32] Li X, Gao H, Murphy C J and Caswell K K 2003 *Nano Lett.* **3** 1495
[33] Palaci I, Fedrigo S, Brune H, Klinke C, Chen M and Riedro E 2005 *Phys. Rev. Lett.* **94** 175502
[34] Yu M F, Lourie O, Dyer M J, Moloni K, Kelly T F and Ruoff R S 2000 *Science* **287** 637
[35] Stan G and Price W 2006 *Rev. Sci. Instrum.* **77** 103707
[36] Hutter J L and Bechhoefer J 1993 *Rev. Sci. Instrum.* **64** 1868